Journal Pre-proofs

Nanoparticles decorated carbon nanotubes as novel matrix: A comparative study of influences of immobilization on the catalytic properties of Lens culinaris β-galactosidase (Lcβ-gal)

Anjali Yadav, Dinesh Chand Agrawal, Rohit Ranjan Srivastava, Anchal Srivastava, Arvind M. Kayastha

PII: S0141-8130(19)35758-7
DOI: https://doi.org/10.1016/j.ijbiomac.2019.09.194
Reference: BIOMAC 13475

To appear in: *International Journal of Biological Macromolecules*

Received Date: 24 July 2019
Revised Date: 24 September 2019
Accepted Date: 24 September 2019

Please cite this article as: A. Yadav, D. Chand Agrawal, R. Ranjan Srivastava, A. Srivastava, A.M. Kayastha, Nanoparticles decorated carbon nanotubes as novel matrix: A comparative study of influences of immobilization on the catalytic properties of Lens culinaris β-galactosidase (Lcβ-gal), *International Journal of Biological Macromolecules* (2019), doi: https://doi.org/10.1016/j.ijbiomac.2019.09.194

Nanoparticles decorated carbon nanotubes as novel matrix: A comparative study of influences of immobilization on the catalytic properties of Lens culinaris β-galactosidase (Lcβ-gal)

Anjali Yadav[a], Dinesh Chand Agrawal[a], Rohit Ranjan Srivastava[b], Anchal Srivastava[b], Arvind M. Kayastha[a]*

[a]*School of Biotechnology, Institute of Science, Banaras Hindu University, Varanasi, 221005, India.*
[b]*Department of Physics, Institute of Science, Banaras Hindu University, Varanasi, 221005, India.*

[*] *Corresponding Author: kayasthbhu@gmail.com*
Phone number: +919451000575 (Arvind M. Kayastha)

Keywords: β-galactosidase, Nanobiocatalysts, Nanocomposites

Abstract

In the present study, Multiwalled carbon nanotubes (MWCNT) decorated with two different nanoparticles namely tungsten disulfide (WS_2) and tin oxide (SnO_2), nanocomposites (NCs) were synthesized via hydrothermal methods. Spectroscopic studies showed that both synthesized NCs possess nearly same functional groups but MWCNT-SnO_2 NCs are rich in O-functional group. Microscopic studies revealed that both NCs have different morphological microstructure. *Lens culinaris β*-galactosidase (*Lcβ-gal*) was immobilized using glutaraldehyde cross-linker resulted in immobilization efficiency of 91.5% and 88 % on MWCNT-WS_2 and MWCNT-SnO_2 NCs, respectively. Remarkable increase in rate of hydrolysis of whey lactose has been observed with both NCs i.e. *Lcβ-gal* immobilized MWCNT-WS_2 hydrolyzes the 97% whey lactose in 1.5 h while MWCNT-SnO_2 showed maximum 92% of whey hydrolysis in 2 h at optimum condition. Both nanobiocatalyst could serve as a promising candidates for dairy industries and would offer a potential platform for enzyme based biosensor fabrication.

1. Introduction

Nowadays, enzymologist have shown their exceptional interest in enzyme catalysis because of their diverse applications in various fields such as food industry [1], textile [2], paper pulp [3], cosmetics [4], fine chemical synthesis [5], and pharmaceuticals industries [6, 7] etc. Major advantage of enzyme catalysis is

that it plays a crucial role towards green and sustainable industrial development [8, 9]. But, soluble enzymes possess some serious drawbacks that limits their applications such as they are extremely sensitive to industrial conditions like higher temperature, pH variations, shearing forces, and organic solvents, which affects their bioconversion efficiency as compared to *in vivo* conditions [10, 11]. Immobilization technology provides a potential platform to re-engineer the biocatalyst with enhanced properties which tremendously increases the thermal stability, broadens the operational pH and temperature working range, boosts resistance to various organic solvents and also prevents product inhibition etc. Apart from these properties, it also increases the reusability of the expensive biocatalyst which allows simplistic separation of products from reaction mixture [12, 13].

Nanotechnological approach to immobilize biocatalyst on diverse scaffolds such as graphene, graphene oxide, iron oxide, carbon nanotubes, and nanowire has gained momentum because of their widespread applications in the field of biomedical engineering, tissue engineering, drug delivery [14], gene therapy [14], and biosensor technology [15, 16]. Recently, carbon nanotubes (CNTs) and many other two dimensional (2D) transition metals such as tin oxide (SnO_2), tungsten disulfide (WS_2), molybdenum disulfide (MoS_2), and manganese dioxide (MnO_2) have grabbed attention due to their high chemical and mechanical stability, large surface area, biocompatibility and enhanced electrical properties [17, 18]. In the past, our laboratory explored nanomaterials such as graphene nanosheets [19], MoS_2 nanosheets [20], iron oxide, and graphene oxide [21] with successful

immobilization of enzymes onto them. But, these 2D nanomaterial showed some shortcomings such as poor solubility in water and buffers, and often tend to aggregate due to their high active surface area which further reduced the surface to volume ratio and hence reduces enzyme loading capacity [22]. Furthermore, aggregation of 2D nanomaterial leads to structural deformation, resulting in reduced electrical conductivity [22].

Three dimensional (3D) nanocomposites have emerged as a solution to conquer the inadequacies associated with these nanomaterials. 3D nanocomposites have been synthesized in which CNTs were incorporated in between nanoparticles/nanorods to prevent the alteration in volume change. Recently, we have successfully immobilized β-galactosidase onto MWCNT-MoS_2 nanocomposite with immobilization efficiency of 93% [23]. Asmat and Husain [24] have successfully fabricated various nanocomposites such as nanocellulose fused polypyrrole/graphene oxide nanocomposites, poly(o-toludine) functionalized nanocomposites [25], polyamine grafted MWCNTs impregnated with cobalt [26], and polyprrole-methyl anthranilate functionalized worm like titanium oxide [27] for immobilization of lipase. In all the cases, exquisite stability and catalytic performance was observed. These nanocomposites contain porous network structure, which provide larger surface area for attachment of biocatalyst and also facilitates the diffusion of substrate to the enzyme and release of product. These nanocomposites due to their excellent electrical property are more acquiescent for fabrication of biosensor for sensitive detection and recognition of different biomolecules.

β-Galactosidases (EC.3.2.1.23) also known as lactases are well-known for the hydrolysis of lactose sugar present in milk and other dairy products [28]. Milk and dairy products are essential component of human diet but when the consumption of milk exceeds over the residual activity of *β*-galactosidase left in small intestine where undigested lactose passes in large intestine and fermented by colonic microflora causing several symptoms like abdominal pain, loose stool, nausea etc. [28, 29]. According to a report, lactose intolerance prevails about 70% of world population. Therefore, lactose intolerant people are advised to take lactose reduced or lactose free dairy products. Hydrolytic property of *β*-galactosidase has been exploited by dairy industry as a solution for the production of lactose free/reduced dairy products [29, 30]. However, it also unravel the problem of formation of ice crystals in dairy products (ice cream) by addition of *β*-galactosidase and subsequently, it also enhances the sweetness and flavor of dairy products [31, 32]. It also owns the property of recycling the waste of cheese industry by bioconversion of whey in ethanol, and other value added products. Transgalactosylation property of *β*-galactosidase has been utilized by dairy industries in production of Galacto-oligosaccharides (GOS) which is of great biotechnological implications [33]. GOS act as prebiotic which help in maintaining the microflora of intestine and improve the immune system. The tremendous industrial applications of *β*-galactosidase has motivated us to choose this enzyme and followed by its immobilization onto nanocomposites (NCs) such as multiwalled carbon nanotubes-tungsten di sulfide (MWCNT-WS_2) and multiwalled carbon nanotubes-tin oxide (MWCNT-SnO_2).

In present work, two different NCs i.e. MWCNT-WS_2 and MWCNT-SnO_2 were synthesized *via* facile hydrothermal method. *β*-Galactosidase from *Lens culinaris* (*Lcβ-gal*) was immobilized onto these nanocomposites using glutaraldehyde cross-linker *via* covalent bond formation as shown in **Scheme 1**. Atomic Force Microscopy (AFM), Field Emission-Surface Electron Microscopy (FE-SEM), Fourier Transformed Infrared region (FTIR), Confocal Laser Scanning Microscopy (CLSM) have been employed for characterization of both nanobiocatalyst (NBCs). In both cases, Response Surface Methodology (RSM) has been employed to optimize various parameters to get maximum immobilization. A comparative study of biochemical and kinetics parameters has been carried out for both nanobiocatalyst (NBCs). The NBCs, could be serve as a promising candidate for treatment of waste produced by dairy industry, before discharging into water bodies.

2.0. Experimental Section

Tin chloride pentahydrate ($SnCl_4.5H_2O$), sodium hydroxide and iso-propyl alcohol were purchased from Molychem, India. Sodium tungstate dihydrate ($Na_2WO_4.2H_2O$) and L-cysteine was purchased from Molychem, India. The chemical reagent used for buffer preparation throughout experiments were of analytical grade, and were procured from Merck Eurolab GmbH Darmstadt, Germany. All the chemicals used during experiments were purchased from Sigma-Aldrich (St. Louis, MO). Milli Q water (Millipore, Bedford, MA) with resistance more 18 MΩ.cm has been used throughout the experiment. *Lens culinaris* seeds were purchased from local market.

2.1. Enzyme extraction

All the purification steps were performed at 4 ℃ and centrifugation was done for 20 min at 7267×*g* at 4 ℃, unless stated otherwise.

Lens culinaris seeds (50 g) were soaked overnight in extraction buffer, homogenized in Waring blender in ratio of 1:2 with sodium phosphate buffer (25 mM, pH 6.7). Thus, crude extract was purified by using published procedure [23].

2.2. Synthesis of multiwalled carbon nanotubes-tin oxide (MWCNT- SnO_2 NCs)

MWCNTs were synthesized by using spray pyrolysis technique as described earlier [34]. The nanocomposite of SnO_2 and MWCNT was synthesized using facile and eco-friendly hydrothermal method. In synthesis process, $SnCl_4.5H_2O$ (3.5 g) was dissolved in isopropyl alcohol further 10 ml of distilled water added to the solution under vigorous stirring condition for 1 h. During stirring, 0.8 M of NaOH was added drop-wise in order to maintain the pH ~12 of the above solution. In the next step, MWCNT (0.5 g) was dispersed into the above solution and stirred vigorously. Further, the complete suspension was transferred into 100 ml of Teflon-lined autoclave and kept into an oven maintained at 180 ºC for 12 h. After natural cooling to room temperature, black colour precipitate was obtained which was separated by centrifugation at 1162×g. Finally the precipitate was washed several times with Milli Q water and dried in oven maintained at 60 ºC, overnight.

2.2.1. Synthesis of multiwalled carbon nanotubes –tungsten disulphide (MWCNT- WS_2 NCs)

The nanocomposite of WS_2 and MWCNT was again prepared by hydrothermal method. In brief, sodium tungstate dihydrate (0.25g) was dissolved in 25 ml of distilled water in a beaker and stirred at room temperature. In another beaker, 0.5 g of L-cysteine was dissolved in 50 ml distilled water. Further, both the solutions were mixed into a beaker and pH of the solution was maintained at 6.5 by adding the HCl (0.1 M) solution into it. In the next step, 0.5 g of MWCNT was dispersed into the above solution and ultra-sonicated for 1 h. Finally, the mixture was transferred into 100 ml of Teflon-lined autoclave and kept into an oven maintained at 200 ºC for 48 h. After natural cooling to room temperature, black color precipitate was obtained which was further centrifuged and washed multiple times with Milli Q and dried at 80 ºC, overnight.

2.2.2. Immobilization of Lcβ-gal onto MWCNT-WS_2 and MWCNT-SnO_2 NCs

Immobilization of *Lcβ-gal* onto functionalized nanocomposite was performed by the following published procedure [23] with minor modification. Similar, protocol was followed for both NCs. Approximately 1 mg/ml of MWCNT-WS_2 and MWCNT-SnO_2 NCs were dispersed in sodium acetate buffer (50 mM, pH 5.0) separately, sonicated for 5 min and centrifuged at 1162×g for 5 min. The pellet thus obtained was incubated with glutaraldehyde (2-5%; v/v) solution, with gentle mixing in dark for 4 h. Thereafter, excess of glutaraldehyde was removed, and washed with chilled sodium acetate buffer. Finally, different amount of enzyme were added to it and left for overnight at 4℃. Next day, unbound enzyme was removed by washing twice with chilled buffer.

2.3. Protein estimation

Protein was estimated according to Bradford method [35] by using bovine serum albumin (BSA) as a standard.

2.4. Enzyme assay

The activity of *β*-galactosidase was monitored by using the published procedure as described earlier by Yadav et al. [23] with some modification. The hydrolytic activity of *Lcβ-gal* was determined by assessing the release of o-nitrophenol from *o*, nitrophenyl *β*-D-galactopyranoside (ONPG) at 405 nm. The reaction was carried out in total volume of 500 µl containing suitably diluted enzyme (10 µl) and 490 µl of 20 mM ONPG prepared in Gly-HCl buffer (pH 3.0, 50 mM) at 58 ℃ for 10 min. Further, reaction was stopped by adding 1.5 ml of 20 mM sodium tetra-borate.

One unit of *β*-galactosidase activity is defined as the amount of enzyme required to release 1.0 µmoles of *o*, nitrophenol per min under standard assay conditions (ε 4500 L $mol^{-1}cm^{-1}$).

In case of immobilized enzyme the reaction mixture was centrifuge at 654×g for 1 min and supernatant obtained was analyzed for the formation of *o*, nitrophenolate at 405 nm.

Finally, Immobilization efficiency (%) was calculated using formula:

$$\frac{Specific\ activity\ of\ immobilized\ enzyme}{Specific\ activity\ of\ soluble\ enzyme} \times 100$$

Specific activity of immobilized enzyme was calculated by subtracting the specific activity of unbound enzyme, from the specific activity of loaded enzyme at start of the reaction. While the specific activity of purified sample was 87 U/mg.

2.5. Experimental design and statistical analysis

Box-Behnken Design (BBD) was employed to study the effect of various parameters on response (immobilization %). A few preliminary experiments were carried out to determine the effect various factors affecting response (data not shown). Based on the data of these experiments, various factors (pH, amount of glutaraldehyde (v/v; %), amount of enzyme (μg), amount of NCs (MWCNT-WS_2, MWCNT-SnO_2) affecting the response (immobilization %) were analysed. After analysing initial parameters, BBD generates 29 trials of experiments. The independent factors and their level selected for maximum immobilization of *Lcβ-gal* on MWCNT-WS_2 and MWCNT-SnO_2 as follows:

MWCNT-WS_2 NCs: amount of MWCNT-WS_2 (500 µg, 1000 µg, 1500 µg), glutaraldehyde (v/v; %) (2.5, 3.0, 3.5), pH (4.5, 5.0, 5.5), amount of enzyme (150 µg, 300 µg, 450 µg).

MWCNT-SnO_2 NCs: amount of MWCNT-SnO_2 (500 µg, 1000 µg, 1500 µg), glutaraldehyde (v/v; %) (2.5, 3.0, 3.5), pH (4.5, 5.0, 5.5), amount of enzyme (150 µg, 300 µg, 450 µg).

All the experiments were carried out in triplicates, and their mean values were used for calculation of immobilization (%). BBD design were generated by Design Expert software (version 11, Stats-Ease inc., Minneapolis, MN). The

quadratic polynomial equation has been used to determine the mathematical relationship between independent variable on dependent parameter i.e. response is shown below:

$$Y_i = \beta_\circ + \sum \beta_i X_i + \sum \beta_{ii} {X_i}^2 + \sum \beta_{ij} X_i X_j$$

Y_i represents predicted response, X_i, X_j are input variables which influence the response: $\beta_\circ$ is offset term; β_i is the ith term linear coefficient; β_{ii} is the ith quadratic coefficient and β_{ij} is ijth interaction coefficients. In order to check adequacy and precision of the generated models, statistical evaluation have been carried out by analysing various parameters such as analysis of variance (ANOVA), lack of fit, F value, p value and correlation coefficient R to measure the goodness of fit. The generated model was validated experimentally by performing 29 sets of trial experiments.

2.6. Characterization

To determine the crystallinity of synthesized NCs i.e. MWCNT-WS_2 and MWCNT-SnO_2 has been carried out using X-ray diffractometer (XRD, Philips Pan analytical X'Pert PRO). Spectroscopic characterization of synthesized NCs i.e. MWCNT-WS_2 and MWCNT-SnO_2 was carried out using Raman (Renishaw, inVia, Germany). Microstructural characterization of both NCs i.e. MWCNT-WS_2 and MWCNT-SnO_2 NCs were performed by using Transmission Electron Microscopy (TEM, TECNAI 20G, 200KV). For TEM analysis, respective NCs were dissolved in buffer and sonicated for 30 min, until homogenous solution was obtained. Thereafter, one drop of homogenous solution was loaded onto the

copper grid and air-dried for analysis. To examine the morphological changes before and after the immobilization, Field Emission-Scanning Electron Microscopy (FE-SEM) was employed. Samples were dried and loaded onto the silver glued metallic stub for analysis. In order to ensure the presence of functional group on nanocomposite as well as to get insight into the interaction between nanocomposite and enzyme, FTIR analysis was carried out using Perkin-Elmer (Spectrum 100, USA) spectrophotometer. Samples were mixed with KBr, and obtained pellet was used for analysis and spectra were recorded in 400-4500 cm^{-1} range. Atomic Force Microscopy (AFM) was carried out to study the topological modification before and after immobilization *via* nanoscope (NT-MDT, NIGERA, PRIMA model, Russia), equipped with silicon tip in semi contact mode. For sample preparation, homogenous samples were loaded onto silicon wafer by spin coating method and further, different area were scan with scanning rate of 0.5 Hz. Confocal Laser Scanning Microscopy (CLSM) was employed to examine the distribution of enzyme after immobilization of *Lcβ-gal* onto NCs as well as to confirm immobilization. Fluorescein isothiocyanate (FITC) was labeled to immobilized *Lcβ-gal* on respective NCs and bare nanocomposites as follows: FITC (0.5 mg/ml) was dissolved in dimethyl formamide (DMF) and rest of the volume was made up by extraction buffer and FITC solution (100 µl) was added to bare MWCNT-WS_2, MWCNT-SnO_2 NCs and *Lcβ-gal* immobilized NCs, and incubated for 30 min. Thereafter, excess of FITC solution was removed by washing with MQ water. The laser wavelength at 490 nm was used for excitation.

2.7. Steady state kinetics

2.7.1. Effect of pH

In order to determine optimum pH for the soluble and the immobilized enzyme (MWCNT-WS_2 and MWCNT-SnO_2) w.r.t. ONPG were carried out in pH range 2.5-7.0 (Glycine-HCl buffer pH 2.5-4.0; sodium acetate buffer 4.0-5.5; sodium acetate buffer 5.5-7.0), 50 mM each. The activity at pH 3.0 was taken as control (100%) for calculation of remaining activity.

2.7.2. Effect of temperature and thermal stability

Evaluation of optimum temperature was carried out in temperature range 25 ℃ to 75 ℃ for soluble and immobilized (MWCNT-WS_2 and MWCNT-SnO_2) at its optimum pH w.r.t. ONPG. Thermal stability studies of enzyme were carried out by incubating soluble and immobilized (MWCNT-WS_2 and MWCNT-SnO_2) enzyme at different temperature for different time intervals; aliquots were withdrawn at regular time intervals, chilled in ice and assayed for enzyme activity.

2.7.3. Determination of K_m

Lineweaver-Burk Plot has been employed to study K_m of *Lcβ-gal* for soluble and immobilized enzyme, by varying the substrate concentrations from 0.2 mM to 20 mM. Data were plotted and analysed using Sigma plot version 11.

2.7.4. Storage stability and reusability

The aliquots of soluble enzyme and NBCs (MWCNT-WS_2 and MWCNT-SnO_2) were stored at room temperature under dry and wet conditions at 4 ℃ in sodium phosphate buffer (25 mM, pH 6.8) for different time intervals. Assessment of

residual activity was carried out at regular intervals w.r.t. ONPG as a substrate. However, to check the reusability respective NBCs (MWCNT-WS_2 and MWCNT-SnO_2) were repeatedly used for the assessment of residual activity with both NBCs w.r.t. ONPG in 48 h. After each assay, the NBCs was washed repeatedly with sodium acetate buffer (50 mM, pH 5.0). The activity determined at first step was taken as control (100%) to calculate rest of the activity.

2.7.5. Cytotoxicity of nanobiocatalyst

Murine lymphoma cell line designated as Dalton Lymphoma (DL) were placed in 96-well tissue culture plate (1×10^6/well) alone and with NBCs at various concentration (25-150 µg) for 24 h at 37 ℃ in 5% CO_2 incubator. Next, standard 3-(4,5-dimethylthiazol-2-yl)-2,5-diphenyl tetrazolium-bromide (MTT) assay was performed as described earlier Yadav et al. [36] with minor modification. Briefly, MTT solution (5 mg/ml) prepared in Phosphate Buffer Saline (PBS) was added to the 96-well tissue culture plate and incubated for 4 h. Thereafter, plate was centrifuged at 10×g. The supernatant was aspirated without disturbing dark blue formazan crystal generated by live cell. The absorbance was measured at wavelength of 540 nm using a microplate reader. The cytotoxicity analysis of both NBCs were carried out separately. The experiments were performed in triplicates for all test concentration of NBCs.

2.7.6. Whey hydrolysis

Whey hydrolysis was monitored for the formation of glucose by using glucose oxidase-peroxidase coupled assay procedure (GOD-POD kit) (Surat, India). Preparation of milk whey has been carried out by following protocol with minor

modification, as described earlier by Dwevedi and Kayastha [37]. In brief, milk pH was brought down to pH 4.5 with 1N HCl, followed by centrifugation for 10 min at 8420g, and 4 ℃. Whey supernatant (100 µl) was incubated with respective NBCs (1 mg) (MWCNT-WS_2 and MWCNT-SnO_2 NCs) for 24 h at room temperature and 55 ℃. From above reaction mixture 20 µl was withdrawn at regular time intervals for the assessment of released glucose at 505 nm.

3.0. Results and Discussion

Lcβ-gal has been purified to electrophoretic homogeneity with 857 fold and a specific activity of 87 U/mg by using different fractionation and chromatography steps [23].

3.1. Structural and microcrystal characterization

To determine the crystallinity of as synthesized MWCNT-SnO_2 and MWCNT-WS_2 NCs were characterized by X-ray diffractometer. In **[Fig. 1(a)]**, the characteristics diffraction peaks of SnO_2 were observed at 26.8º, 29.7º, 31.8º, 33.8º, 40.6º, 44.5º, 51.7º, 56.4º,58.0º, 66.4º, 71.2º, and 75.5º which corresponds to diffraction plane (112), (113), (021), (006), (123), (101), (130), (028), (119), (042), (143), and (145), respectively. The diffraction peak observed at 26.09º corresponds to (00.2) plane of MWCNT. The XRD pattern of SnO_2 and MWCNTs nanocomposite are matches well with JCPDS card no. 78-1063 and 75-1621, respectively**.** The additional peak of Sn was observed at 32.0º, which corresponds to the diffraction plane (200) suggesting that small amount of $SnCl_4.5H_2O$ was not converted into SnO_2 during the reaction process. In **[Fig. 1(b)]**, the characteristic peaks of WS_2 were observed at 14.3º, 33.5º, 39.5º, 49.7º,

58.3º, 60.5º and 73.0º, which correspond to diffraction plane (100), (101), (103), (105), (110), (112) and (203), respectively. In this case again characteristics peak of MWCNT are observed at 26.09º and 44.00º, which corresponds to diffraction plane (00.2) and (101), respectively. The XRD pattern of prepared WS_2 and MWCNTs NCs matches well with JCPDS card no. 08-0237 and 75-1621, respectively.

Raman spectroscopy is a very versatile and non-destructive technique to determine the vibrational modes of any materials. Therefore, synthesized MWCNT-SnO_2 and MWCNT-WS_2 NCs have been characterized through Raman spectroscopy technique. The Raman spectrum of MWCNT-SnO_2 composite shown in **[Fig. 1(c)]**, consists of two bands at 560 cm^{-1} and 630 cm^{-1}, which corresponds to Sn-O surface vibrations and A_{1g} (out of plane) vibration mode, respectively [38]. The Raman spectrum of MWCNT-WS_2 composites shown in **[Fig. 1(d)]**, consists of two characteristics peaks 351 cm^{-1} and 421 cm^{-1}, which are assigned to E^1_{2g} (in plane) vibrational mode and A_{1g} (out of plane) vibrational mode, respectively [39]. Few, additional peaks have also been observed with peak values 323 cm^{-1}, 521 cm^{-1} and 585 cm^{-1}, which correspond to E_{1g}, E^1_{2g} + LA and A_{1g} + LA vibrational modes, respectively [40]. In the Raman spectra of both MWCNT- SnO_2 and MWCNT-WS_2 composites, peaks observed at 1346 cm^{-1} and 1577 cm^{-1} correspond to D band and G band of MWCNT, respectively. The D band signifies the disorderness and defects in the finite crystal size whereas G band is assigned to E_{2g} tangential mode and graphitic nature with sp_2 hybridization of MWCNT. The peak observed at 2730 cm^{-1}, corresponds to the

2D band of MWCNT, which is also referred as the first overtone of D band [41]. Hence, Raman spectrum clearly confirms the successful synthesis of MWCNT-SnO_2 and MWCNT- WS_2 nanocomposites.

Microcrystal and structural characterization of NCs was studied using TEM. In the present study, the morphological characterization of MWCNT, MWCNT-WS_2 NCs, and MWCNT-SnO_2 NCs has been carried out. TEM micrograph of MWCNT **[Fig. 2(a)]** clearly showed multiple small tube within tube like structure, which further confirmed the formation of MWCNTs. **[Fig. 2(b)]** demonstrates agglomeration of SnO_2 nanoparticles over the surface of MWCNT and it showed that SnO_2 nanoparticles (NPs) owns circular structure. From **[Fig. 2(c)]** it is evident that WS_2 possess nano-rod like structure in which rod end, into triangular structure, followed by the attachment of WS_2 nano-rods onto MWCNTs (highlighted by blue dotted circle).

The detailed morphological changes of synthesized NCs i.e. MWCNT-WS_2 and MWCNT-SnO_2 before and after immobilization were studied using FE-SEM **[Fig. 3]**. Native MWCNT-WS_2 NCs **[Fig. 3(a)]** revealed that MWCNTs are interconnected to each other which leads to formation of network like structure, wrapped by WS_2 nanorods (highlighted with yellow colour). Non-uniform distribution of WS_2 nanoflower can be seen over the surface of CNT-WS_2 while synthesized NBCs **[Fig. 3(b)]** showed that these MWCNT rods are coalesce along with dense coverage of enzyme over the surface of NBCs. However, a significant increase in the thickness of diameter of CNT rods were observed, shown in **supplementary material [S1]**. Native MWCNT-SnO_2 **[Fig. 3(c)]** revealed that

fewer MWCNTs as compared to MWCNT-WS_2. SnO_2 nanoparticle are agglomerated onto the surface of MWCNTs rods, which resulted in non-uniform distribution of SnO_2 nanoparticles on the surface of synthesized NCs. However, after immobilization **[Fig. 3(d)]** coalesced of enzyme and NCs was observed along with increase in the thickness of CNTs rods, which ensures the successful immobilization.

The immobilization and distribution of enzyme over the surface of nanocomposites was examined *via* CLSM as shown in **[Fig. 4**]. **[Fig. 4 (a & c)]** represents the native MWCNT-WS_2 and MWCNT-SnO_2 NCs in which no FITC signals were observed, which indicated that there is no enzyme while laser scanning at 63x yielded fluorescent image **[Fig. 4(b)]** showed non-uniform distribution of FITC signal in which CNTs rod are covered by FITC labeled enzyme (highlighted by yellow color) while at few places strong FITC signal can be observed that might be probably due to immobilization of *Lcβ-gal* onto MWCNT-WS_2 NCs. However, in case of MWCNT-SnO_2 **[Fig. 4(d)]** different FITC signal was observed which showed a dense coverage of enzyme over the surface of NCs. This can also be confirmed by FE-SEM micrograph **[Fig. 3(d)]** in which after immobilization only a few MWCNT rods are evident as compared to SnO_2 nanoparticles.

AFM has become one of the benchtop techniques in laboratory due to its potential application in measuring, analyzing and imaging the biomolecules and bio-surfaces with higher resolution at nanoscale level [42]. Therefore, AFM was

carried out to examine the surface topological modification before and after the immobilization. Topological micrograph of native MWCNT-WS_2 NCs **[supplementary material Fig. S2(a)]** demonstrated the homogenous distribution of nanocomposites in which MWCNTs and WS_2 nano-rods were observed (highlighted with yellow dashed circle) over complete scanning area of 3µm×3µm. In 3D view, **[supplementary material Fig. S2(b)]** WS_2 nano-rods were observed over MWCNT in the form of crest and tough. The height of bare nanocomposite has approximately 40 nm. However, after immobilization jagged transparent patches of immobilized enzyme can be seen over surface of nanocomposites as shown in 2D view in scanning area of 10µm×10µm with increase in the average height after immobilization approximately 400 nm and it can also be seen as white spikes over surface of NCs in 3D view **[supplementary material Fig. S2(c & d)]**.

While in case of native MWCNT-SnO_2 NCs **[supplementary material Fig. µS3(a)]** agglomeration of nanoparticles can be seen over the surface of NCs in 2D view and it resulted in different height with average thickness of 40 nm in 3D view over the scanning region of 3µm×3µm **[supplementary material Fig. S3(b)]**. However, after immobilization of enzyme on NCs, transparent uneven distribution of white patches of enzyme can be seen over the surface of MWCNT conjugated to nanoparticles with increase in average thickness of 600 nm over the scanning area of 20µm×20µm (highlighted with blue dashed line). Besteman et al. [43] also observed similar result when glucose oxidase was immobilized on the single walled carbon nanotubes.

3.2. Optimization

Before setup of any process, optimization is an essential parameter from industrial perspective because it doesn't only aid us to select favourable conditions to achieve best performance of the system but it also reduces the cost of doing extensive laboratory work, and saves time [44]. BBD has been found to be more proficient and precise as compared to CCD. Therefore, in the present study BBD has been applied with both NCs, MWCNT-WS_2 and MWCNT-SnO_2 to optimize the immobilization process. Results obtained from preliminary experiments have been employed to optimize various parameters in operational range such as pH, glutaraldehyde (%; v/v), amount of enzyme, amount of nanocomposites with both NCs i.e. MWCNT-WS_2 and MWCNT-SnO_2 to get maximum response are shown in **supplementary material [Table S1 & Table S2]**. The actual factor which affects the immobilization are represented in terms of equations are as follows. With both NCs, MWCNT-WS_2 and MWCNT-SnO_2 NCs different contour and their respective 3D plot were designed showing the interaction effect on the response (immobilization) shown in **supplementary material [Fig. S4]** and the following were determined:

In case of MWCNT-WS_2:

Amount of MWCNT-WS_2: 1074.16 µg; pH: 4.94; glutaraldehyde: (v/v; %) 3.08; amount of β-gal: 348.68 µg; predicted immobilization 90.81%

In case of MWCNT-SnO_2:

Amount of MWCNT-SnO_2: 849.92 µg; pH: 5.20; glutaraldehyde: (v/v; %) 3.27; amount of β-gal: 365.58 µg; predicted immobilization 86.82%

To validate the above predicted immobilization, a few experiments were carried out with both NCs and 91.5% and 88% immobilization was achieved with MWCNT-WS_2 and MWCNT-SnO_2, respectively. The values were found to be in close agreements with the predicted values and equation as given below,

Immobilization efficiency: MWCNT-WS_2 NCs:

$$-473.69200+0.0379 \times A+150.00 \times B+99.79 \times C+0.113132 \times D+0.002A \times B-0.000400A \times C+0.000015A \times D-6.100 \times B \times C-0.0133B \times D+0.028100 \times C \times D-0.000024 \times A^2-13.01900 \times B^2-12.83400 \times C^2-0.0002$$

whereas A; represents amount of MWCNT-WS_2, B; pH, C; Glutaraldehyde (%; v/v), D; amount of enzyme

MWCNT-SnO_2 NCs:

$$-428.66 + 0.0663583 \times A + 114.967 \times B + 107.483 \times C + 0.0711944 \times D + -0.00133 \times A \times pH + -0.012 \times A \times C + 3.66667e\text{-}06 \times A \times D + 6 \times B \times C + 0.0212333 \times B \times D + -0.00166667 \times C \times D + -1.10517e\text{-}05 \times A^2 + -13.3867 \times B^2 + -20.0167 \times C^2 + -0.000258352 \times D^2$$

A; represents the amount of MWCNT-SnO_2, B; pH, C; glutaraldehyde (%; v/v), D; amount of enzyme

To check the significance of the model, ANOVA was performed with both NCs i.e. MWCNT-WS_2 and MWCNT-SnO_2. With both NCs, the model p-value <0.0001 showed that model terms are significant. The model F-value 50.62 and 41.32 in case of MWCNT-WS_2 and MWCNT-SnO_2, respectively implies that model is significant and there is only 0.01% chances that large F-value may occur

due to noise shown in **supplementary material** [**Table S3]**. Another parameter, lack of fit is also important to measure the fitness of the model, non-significant lack of fit showed that model was valid for the present study. However, in case of MWCNT-WS_2, F-value of lack of fit is 1.39 which implies that lack of fit is not significant to relative pure error means there is only 40.25% chances that large lack of fit could have occurred due to noise. In case of MWCNT-SnO_2, lack of fit F-value 3.28 indicates that the model is non-significant and there is only 13.17% chance that large non-significant lack of fit due to noise. Adequate precision shows signal to noise ratio, a ratio of 4 is required for good model. In the present study the ratio of 22.895 and 21.448 in case of MWCNT-WS_2, MWCNT-SnO_2, respectively was achieved which indicated the reliability of the experimental data. Predicted R^2 measures accuracy of the model with which it predicts the response value (immobilization). A difference of less than 0.2 is required between adjusted and predicted R^2.

In the present study, predicted R^2 is in reasonable agreement with adjusted R^2 with both NCs i.e. MWCNT-WS_2 and MWCNT-SnO_2 and both models showed a difference of less than 0.2 **supplementary material** [**Table S4]**. Coefficient of determination R^2 is also a significant parameter, higher R^2 value is pre-requisite for a good model. In case of MWCNT-WS_2, R^2 0.9806 was achieved which indicated that model explains 98.06% of variation of immobilization by independent variables and also implied that only 1.94% variations are not explained by the model. While in case of MWCNT-SnO_2 R^2 is 0.9764 indicating present model explains 97.64% of variation of immobilization by independent

variables but it fails to explain 2.36% of variations only. These results showed that model predicted the immobilization efficiency with high precision value.

To get mechanistic insights into the interaction between nanocomposites and *Lcβ-gal*, FTIR analysis has been carried out, which also enlighten the nature of functional groups present on the nanocomposites. **Supplementary file Fig. S5** shows the vibrational frequencies of MWCNT-WS_2 at 790 cm^{-1}, 1121 cm^{-1}, 1567 $cm^{-1}$and 3410 cm^{-1} corresponds to W-S stretching and bending vibrations, C=N stretching, NH bend of 1^0 amines and –OH stretching of alcohols groups, respectively [45]. These vibrational frequencies ascertains the presence of -N and -O containing functional groups. The FTIR spectrum of MWCNT-SnO_2 confirmed the presence of oxygen containing functional groups, such as C-OH at 3435 cm^{-1}, O-H deformation peak at 1651 cm^{-1}, the C-O stretching peak at 1124 cm^{-1}, and the –CH in plane bending vibration peak at 1400 cm^{-1}[46]. The peaks at 2859 cm^{-1} and 2925 cm^{-1} corresponds to C-H asymmetric stretching of the $–CH_3$ and $–CH_2$ groups. The signature peaks appearing at 516 cm^{-1}, 660 cm^{-1}corresponds to Sn-O asymmetric stretch, and Sn-O-Sn symmetric stretch [47], respectively **[supplementary material Fig. S6].** These results suggested that MWCNT-SnO_2 is rich in -O functionalities. Thereafter, glutaraldehyde was added in both NCs in which one arm of glutaraldehyde binds to –N and –O functional group *via* formation of covalent bond and hemiacetal bond, respectively. The binding of glutaraldehyde to NCs surface was ascertained by the vibrational frequencies appearing at 1626 cm^{-1} and 1664 cm^{-1} in case MWCNT-WS_2 and MWCNT-SnO_2, respectively. There was drastic change in spectra obtained after

immobilization of *Lcβ-gal*. In case of MWCNT-WS_2 a weak band appearing at a frequency of 1616 cm^{-1} showed shift which confirms the stretching of C=O due to formation of carbonyl amide I bond of peptide linkage in enzymes. While in case of MWCNT-SnO_2, frequency at 1634 cm^{-1} showed shift and decrease intensity that ascertains the formation of amide bond between free arm of glutaraldehyde and *Lcβ-gal*, as well as broadening of peak 3234 to 3423 cm^{-1} was observed due to stretching of N-H, which endorses the successful immobilization of *Lcβ-gal* onto nanocomposites. A drastic decrease in intensities were observed with both NCs i.e. MWCNT-WS_2 and MWCNT-SnO_2 that may be due to strong covalent interaction between *Lcβ-gal* and nanocomposites. Similar observation were also made by other researchers [48, 49]

3.3 *Steady state kinetics*

3.3.1. Effects of pH

Nanoenviornmental conditions govern the shift in optimum pH of the immobilized enzymes. In the present study, NBCs showed no shift in optimum pH when immobilized with MWCNT-WS_2 NCs while in case MWCNT-SnO_2, NBCs showed a shift of one unit in optimum pH towards alkaline pH. However, in both cases broadening in pH profile was observed as compared to soluble *Lcβ-gal*. It retained 85% and 75.4% of residual activities with both NCs i.e. MWCNT-WS_2 and MWCNT-SnO_2, respectively, at pH 2.5 which is good as compared to soluble *Lcβ-gal* activity at the same pH **[Fig. 5(a)]**. While at pH 7.0 the synthesized NBCs retained 58% and 56% of residual activities with MWCNT-WS_2 and MWCNT-SnO_2, respectively as compared to soluble *Lcβ-gal* which had

retained only 25% of residual activity at same pH **[Fig. 5(a)]**. Verma et al. [50] had also investigated shift in optimum pH after immobilization of *β*-galactosidase from *Kluyveromyces lactis* onto the silicon oxide nanoparticles. However, the degree of the shift in optimum pH varies with nature of matrices used. It depends upon the type of charge owned by nanocomposite that influences the proton gradient which alters the pH value in near vicinity of the enzymes. Significant broadening in pH profile at higher temperature with enhanced activity of both synthesized NBCs has made them an auspicious candidate for food industries.

3.3.2. Optimum temperature and thermal stability

Optimum temperature studies of both NBCs showed a shift of one degree from soluble *Lcβ-gal* **[Fig. 5(b)]**. After reaching temperature optima, a sharp decline in activity was observed with soluble *Lcβ-gal* after 58 ℃. Both NBCs showed higher activity and higher tolerance at elevated temperature and also showed widening of operational temperature range. The soluble *Lcβ-gal* retained only 27% of activity at 70 ℃ while the synthesized NBCs retained 70% and 65% residual activities with MWCNT-WS_2 and MWCNT-SnO_2 NCs, respectively at same temperature. Das et al. [21] also explored shift in temperature optima when *β*-amylase was immobilized onto graphene oxide and graphene oxide-CNT.

Industrial quest of thermostable enzymes are still prominent area of research. Generally, industries operate at higher temperature thus thermostability of enzymes becomes a crucial parameter. In the present study, when *Lcβ-gal* immobilized MWCNT-WS_2 was incubated at 55 ℃ for 2 h, it retained 96.6% of residual activity while MWCNT-SnO_2 retained 92.4% of residual activity under

similar conditions. Thermal stability of both the NBCs was also tested at 60 ℃, which revealed that *Lcβ-gal* immobilized MWCNT-WS_2 retained 94.3% of residual activity after 1 h, while MWCNT-SnO_2 retained 87.4% of residual activity under similar condition. However, soluble *Lcβ-gal* retained only 20% of residual activity at 55 ℃ for 2 min. Covalent bond formation results in multipoint attachment between enzyme surface and nanocomposite which makes *Lcβ-gal* more resistant and rigid to unfolding of 3D structural conformation at higher temperatures [51]. Pan et al. [52] also reported enhanced thermal stability of *β*-galactosidase immobilized with magnetic Fe_3O_4-chitosan nanoparticles in the temperature range 50-60 ℃. Such a tremendous increase in thermal stability after immobilization makes these NBCs suitable for cheese whey hydrolysis to minimize the water pollution due to waste produced from cheese industries.

3.3.3. Reusability and storage stability

Shipment of product from the date of manufacturing to end user with retention of biological activity is crucial parameter from industrial viewpoint [53]. Therefore, storage stability or shelf-life study of NBCs is of great relevance for food industries. In the present study, synthesized NBCs retained 90% and 84% in residual activity with MWCNT-WS_2 and MWCNT-SnO_2 NCs, respectively at 4 ℃ over a period of 3 months as shown in **[Fig. 5(d)]**. While the soluble *Lcβ-gal* retained only 30% of the residual activity under similar conditions. The attachment of enzyme to solid supports in proper orientation retained the activity of enzymes over a long period. The remarkable upswing in storage stability of

synthesized NBCs endows valuable candidate for hydrolysis of cheese whey in dairy industries.

Multistep process involved in the purification of enzyme makes it expensive for industrial setup [54]. Therefore, immobilization of enzymes on various matrices have become best alternative to reduce the cost of enzymes by increasing its repeated use. In the present study, both nanocomposites can be reused 9 times, while the MWCNT-WS_2 retained approximately 70% of residual activity after 9^{th} use and MWCNT-SnO_2 NCs showed residual activity of approximately 57% after 9^{th} use **[Fig. 5(c)]**. Retention of activity after several uses may be too strong multipoint covalent attachment of enzyme with NCs, which prevent the detachment of enzyme from NCs [55]. However, repeated use of NBCs resulted in reduced activity that may be due to frequent encountering of substrate to enzyme which leads to distortion of active site present on the enzyme. The obtained results suggested that MWCNT-WS_2 NCs turnout to be more efficient as compared to MWCNT-SnO_2 NCs.

3.3.4. Kinetic parameters

Kinetics parameter of immobilized and soluble *Lcβ-gal* was studied using Lineweaver-Burk plot with ONPG as substrate as outlined in **[Table 1]**. These results suggested that after immobilization, K_m value increases with both NBCs i.e. K_m value of *Lcβ-gal* immobilized MWCNT-WS_2 was 6.75 mM, while in case of MWCNT-SnO_2 was found to be 5.89 mM, respectively. However, K_m value of soluble *Lcβ-gal* was 1.21 mM. Ease of access of substrate toward active site enzyme becomes challenging after immobilization onto nanocomposites, which

leads to higher apparent K_m [54]. Fang et al. [56] also observed increase in K_m after immobilization of laccase onto SiO_2 nanocarrier.

3.3.5 Cytotoxicity of NBCs

In order to ensure the safety of both NBCs (MWCNT-WS_2, MWCNT-SnO_2) in practical usage. The cytotoxic analysis have been carried out using standard MTT assay for both NBCs. MTT assay represents the damage in mitochondrial cells that eventually leads to cell death. The cells were examined for survival *via* standard MTT assay. The results suggested that the both NBCs did not exhibit significant cytotoxicity against DL cells at all test concentrations (25-150 µg/ml).

3.3.6 Whey hydrolysis

The continuous hydrolysis of whey lactose was studied at an analytical scale in batch process under optimum conditions as shown in **supplementary material [Fig. S7(a)]**. *Lcβ-gal* immobilized MWCNT-WS_2 NCs showed maximum 97% of whey lactose hydrolysis in 1.5 h, while *Lcβ-gal* immobilized MWCNT-SnO_2 showed maximum 92% whey lactose hydrolysis at optimum conditions in 2 h. However, for milk lactose the maximum rate of hydrolysis was found to be 72% and 64% in 9 h (data not shown) in case of *Lcβ-gal* immobilized MWCNT-WS_2 and MWCNT-SnO_2 NCs, respectively. **Supplementary material Fig. S7(b)** shows the hydrolysed product i.e. glucose obtained at maximum point of whey lactose hydrolysis. The remarkable increased rate of hydrolysis of whey lactose as compared to milk lactose is due to whey pH optima which lies in acidic range while pH optima of milk lactose lies in alkaline range. Panesar et al. [57] have documented the importance pH optima of whey lactose and milk lactose

hydrolysis. It was observed that prolonged incubation of whey lactose and milk lactose with synthesized nanobiocatalyst did not increases the rate of hydrolysis because, thereafter it attained steady state. Husain et al. [58] have also observed higher rate of lactose hydrolysis in case of whey as compared to milk lactose when *Asperzillus oryzae β*-galactosidase was immobilized onto zinc oxide nanoparticles. Results suggested that *Lcβ-gal* immobilized MWCNT-WS_2 NCs hydrolyzed whey lactose more proficiently as compared to MWCNT-SnO_2 NCs. Therefore, these NBCs could be used as promising candidate in whey lactose hydrolysis in dairy industries at higher temperatures.

4.0. Conclusion

MWCNT-WS_2 NC was found to be superior over MWCNT-SnO_2 NC that may be due to heterofunctional nature. It is evident from reusability and whey hydrolysis test that *Lcβ-gal* immobilized MWCNT-WS_2 showed better reusability and catalytic properties compared to MWCNT-SnO_2. Thus, synthesized NBCs could serve as potential candidate to fulfil the requirement of dairy industries. Apart from this, we hope that present study will provide new insights to explore more novel heterofunctional material to re-engineer the other enzymes based systems with enhanced catalytic properties and would widen their applications such as in bio-catalysis, biosensor technology, and gene delivery etc.

Acknowledgement

Anjali Yadav sincerely expresses her thanks to University Grant Commission, New Delhi for providing financial support in form of Junior and Senior Research Fellowship **(F./2015-16/NFO-2015-17-OBC-UTT-32658/(SA-III-website)**.

Anjali Yadav and Prof. Arvind M. Kayastha are indebted to Prof. S. M. Singh and Mr. Yugal Goel of Animal Cell Culture Laboratory of School of Biotechnology for carrying out cytotoxicity analysis of NBCs on the cell lines maintained in their laboratory. Anjali Yadav is also thankful Mr. Sumit Kumar Pandey for providing MWCNT and Mr. Vijay Kumar Singh for Raman spectra measurements. Rohit Ranjan Srivastava is thankful to UGC for providing fellowship. Anchal Srivastava is grateful to DST, India (DST-PURSE Scheme 5050), CAS-BHU and DST-SERB (EMR/2016/007720) for providing financial assistance.

Conflict of Interests

Authors declare no competing financial interest.

References

[1] P. Fernandes, Enzymes in Food Processing: A condensed overview on strategies for better biocatalysts, Enzyme Research 2010 (2010) 862537.
[2] V.G. Yachmenev, N.R. Bertoniere, E.J. Blanchard, Intensification of the bio-processing of cotton textiles by combined enzyme/ultrasound treatment, Journal of Chemical Technology & Biotechnology 77(5) (2002) 559-567.
[3] P. Bajpai, Application of enzymes in the pulp and paper industry, Biotechnology progress 15(2) (1999) 147-57.
[4] I. Hori, K. Nihei, I. Kubo, Structural criteria for depigmenting mechanism of arbutin, Phytotherapy Research : PTR 18(6) (2004) 475-9.
[5] T. Nagasawa, M. Wieser, T. Nakamura, H. Iwahara, T. Yoshida, K. Gekko, Nitrilase of *Rhodococcus rhodochrous* J1. Conversion into the active form by subunit association, European Journal of Biochemistry 267(1) (2000) 138-44.
[6] H. Griengl, H. Schwab, M. Fechter, The synthesis of chiral cyanohydrins by oxynitrilases, Trends in Biotechnology 18(6) (2000) 252-6.
[7] A.A. Desai, Sitagliptin Manufacture: A compelling tale of green chemistry, process intensification, and industrial asymmetric catalysis, Angewandte Chemie International Edition 50(9) (2011) 1974-1976.
[8] S.J. Benkovic, S. Hammes-Schiffer, A perspective on enzyme catalysis, Science (New York, N.Y.) 301(5637) (2003) 1196-202.
[9] R. Wohlgemuth, Biocatalysis--key to sustainable industrial chemistry, Current Opinion in Biotechnology 21(6) (2010) 713-24.
[10] L. Cao, L.v. Langen, R.A. Sheldon, Immobilised enzymes: carrier-bound or carrier-free?, Current Opinion in Biotechnology 14(4) (2003) 387-394.

[11] R. DiCosimo, J. McAuliffe, A.J. Poulose, G. Bohlmann, Industrial use of immobilized enzymes, Chemical Society Reviews 42(15) (2013) 6437-6474.
[12] W. Tischer, V. Kasche, Immobilized enzymes: crystals or carriers?, Trends in Biotechnology 17(8) (1999) 326-335.
[13] C. Garcia-Galan, Á. Berenguer-Murcia, R. Fernandez-Lafuente, R.C. Rodrigues, Potential of different enzyme immobilization strategies to improve enzyme performance, Advanced Synthesis & Catalysis 353(16) (2011) 2885-2904.
[14] A. Bianco, K. Kostarelos, M. Prato, Applications of carbon nanotubes in drug delivery, Current Opinion in Chemical Biology 9(6) (2005) 674-9.
[15] Q. Zhao, Z. Gan, Q. Zhuang, Electrochemical sensors based on carbon nanotubes, Electroanalysis: An International Journal Devoted to Fundamental and Practical Aspects of Electroanalysis 14(23) (2002) 1609-1613.
[16] R. Singh, A. Yadav, S. Shekhar, R.K. Ajad, R.K. Singh, A.M. Kayastha, Nitrogen doped carbon quantum dots modified by *Lens culinaris* β-Galactosidase as a Fluorescent Probe for Detection of Lactose, Journal of Fluorescence (2019) In press.
[17] J. Kim, J.W. Grate, P. Wang, Nanostructures for enzyme stabilization, Chemical Engineering Science 61(3) (2006) 1017-1026.
[18] W. Feng, P. Ji, Enzymes immobilized on carbon nanotubes, Biotechnology Advances 29(6) (2011) 889-95.
[19] D. Kishore, M. Talat, O.N. Srivastava, A.M. Kayastha, Immobilization of β-galactosidase onto functionalized graphene nano-sheets using response surface methodology and its analytical applications, PLoS One 7(7) (2012) e40708.
[20] R. Das, H. Mishra, A. Srivastava, A.M. Kayastha, Covalent immobilization of β-amylase onto functionalized molybdenum sulfide nanosheets, its kinetics and stability studies: A gateway to boost enzyme application, Chemical Engineering Journal 328 (2017) 215-227.
[21] R. Das, M. Talat, O. Srivastava, A.M. Kayastha, Covalent immobilization of peanut β-amylase for producing industrial nano-biocatalysts: A comparative study of kinetics, stability and reusability of the immobilized enzyme, Food Chemistry 245 (2018) 488-499.
[22] C. Zhu, X. Mu, P.A. van Aken, J. Maier, Y. Yu, Fast Li storage in MoS_2-graphene-carbon nanotube nanocomposites: Advantageous functional integration of 0D, 1D, and 2D nanostructures, Advanced Energy Materials 5(4) (2015) 1401170.
[23] A. Yadav, S.K. Pandey, D.C. Agrawal, H. Mishra, A. Srivastava, A.M. Kayastha, Carbon nanotubes molybdenum disulfide 3D nanocomposite as novel nanoscaffolds to immobilize *Lens culinaris* β-galactosidase (Lsbgal): Robust stability, reusability, and effective bioconversion of lactose in whey, Food Chemistry 297 (2019) 125005.
[24] S. Asmat, Q. Husain, Exquisite stability and catalytic performance of immobilized lipase on novel fabricated nanocellulose fused polypyrrole/graphene oxide nanocomposite: Characterization and application, International Journal of Biological Macromolecules 117 (2018) 331-341.
[25] S. Asmat, Q. Husain, A robust nanobiocatalyst based on high performance lipase immobilized to novel synthesised poly(o-toluidine) functionalized magnetic nanocomposite: Sterling stability and application, Materials Science and Engineering: C 99 (2019) 25-36.
[26] S. Asmat, A.H. Anwer, Q. Husain, Immobilization of lipase onto novel constructed polydopamine grafted multiwalled carbon nanotube impregnated with magnetic cobalt and its application in synthesis of fruit flavours, International Journal of Biological Macromolecules 140 (2019) 484-495.

[27] S. Asmat, Q. Husain, M.S. Khan, A polypyrrole–methyl anthranilate functionalized worm-like titanium dioxide nanocomposite as an innovative tool for immobilization of lipase: preparation, activity, stability and molecular docking investigations, New Journal of Chemistry 42(1) (2018) 91-102.
[28] M. Richmond, J. Gray, C. Stine, Beta-Galactosidase: Review of recent research related to technological application, nutritional concerns, and immobilization1, Journal of Dairy Science 64(9) (1981) 1759-1771.
[29] C. Oliveira, P.M. Guimarães, L. Domingues, Recombinant microbial systems for improved β-galactosidase production and biotechnological applications, Biotechnology Advances 29(6) (2011) 600-609.
[30] P.S. Panesar, S. Kumari, R. Panesar, Potential applications of immobilized & beta-Galactosidase in food processing industries, Enzyme Research 2010 (2010) 16.
[31] T.P. Shukla, L.E. Wierzbicki, Beta- galactosidase technology: A solution to the lactose problem, Critical Reviews in Food Science & Nutrition 5(3) (1975) 325-356.
[32] Q. Husain, β Galactosidases and their potential applications: a review, Critical Reviews in Biotechnology 30(1) (2010) 41-62.
[33] D.P. Torres, M.d.P.F. Gonçalves, J.A. Teixeira, L.R. Rodrigues, Galacto- oligosaccharides: production, properties, applications, and significance as prebiotics, Comprehensive Reviews in Food Science and Food Safety 9(5) (2010) 438-454.
[34] A. Srivastava, O. Srivastava, S. Talapatra, R. Vajtai, P. Ajayan, Carbon nanotube filters, Nature Materials 3(9) (2004) 610.
[35] M.M. Bradford, A rapid and sensitive method for the quantitation of microgram quantities of protein utilizing the principle of protein-dye binding, Analytical Biochemistry 72(1-2) (1976) 248-254.
[36] S. Yadav, S.K. Pandey, A. Kumar, P.K. Kujur, R.P. Singh, S.M. Singh, Antitumor and chemosensitizing action of 3-bromopyruvate: Implication of deregulated metabolism, Chemico-Biological Interactions 270 (2017) 73-89.
[37] A. Dwevedi, A.M. Kayastha, Stabilization of β-galactosidase (from peas) by immobilization onto Amberlite MB-150 beads and its application in lactose hydrolysis, Journal of Agricultural and Food Chemistry 57(2) (2009) 682-688.
[38] S. Yang, Z. Wu, L. Huang, B. Zhou, M. Lei, L. Sun, Q. Tian, J. Pan, W. Wu, H. Zhang, Significantly enhanced dye removal performance of hollow tin oxide nanoparticles via carbon coating in dark environment and study of its mechanism, Nanoscale Research Letters 9(1) (2014) 442.
[39] F. Wang, I.A. Kinloch, D. Wolverson, R. Tenne, A. Zak, E. O'Connell, U. Bangert, R.J. Young, Strain-induced phonon shifts in tungsten disulfide nanoplatelets and nanotubes, 2D Materials 4(1) (2016) 015007.
[40] A. Berkdemir, H.R. Gutiérrez, A.R. Botello-Méndez, N. Perea-López, A.L. Elías, C.-I. Chia, B. Wang, V.H. Crespi, F. López-Urías, J.-C. Charlier, Identification of individual and few layers of WS_2 using Raman Spectroscopy, Scientific Reports 3 (2013) 1755.
[41] T. Odedairo, J. Ma, Y. Gu, J. Chen, X. Zhao, Z. Zhu, One-pot synthesis of carbon nanotube–graphene hybrids via syngas production, Journal of Materials Chemistry A 2(5) (2014) 1418-1428.
[42] N.C. Santos, M.A.R.B. Castanho, An overview of the biophysical applications of atomic force microscopy, Biophysical Chemistry 107(2) (2004) 133-149.
[43] K. Besteman, J.-O. Lee, F.G. Wiertz, H.A. Heering, C. Dekker, Enzyme-coated carbon nanotubes as single-molecule biosensors, Nano letters 3(6) (2003) 727-730.

[44] R.F. Gunst, Response Surface Methodology: Process and product optimization using designed experiments, technometrics 38(3) (1996) 284-286.
[45] J. Wu, G. Yue, Y. Xiao, M. Huang, J. Lin, L. Fan, Z. Lan, J.-Y. Lin, glucose aided preparation of tungsten sulfide/multi-wall carbon nanotube hybrid and use as counter electrode in dye-sensitized solar cells, ACS Applied Materials & Interfaces 4(12) (2012) 6530-6536.
[46] L. Lin, H. Xing, R. Shu, L. Wang, X. Ji, D. Tan, Y. Gan, Preparation and microwave absorption properties of multi-walled carbon nanotubes decorated with Ni-doped SnO_2 nanocrystals, RSC Advances 5(115) (2015) 94539-94550.
[47] A. Kumar, L. Rout, R.S. Dhaka, S.L. Samal, P. Dash, Design of a graphene oxide-SnO_2 nanocomposite with superior catalytic efficiency for the synthesis of β-enaminones and β-enaminoesters, RSC Advances 5(49) (2015) 39193-39204.
[48] A. Deep, U. Tiwari, P. Kumar, V. Mishra, S.C. Jain, N. Singh, P. Kapur, L.M. Bharadwaj, Immobilization of enzyme on long period grating fibers for sensitive glucose detection, Biosensors and Bioelectronics 33(1) (2012) 190-195.
[49] M. Khan, Q. Husain, R. Bushra, Immobilization of β-galactosidase on surface modified cobalt/multiwalled carbon nanotube nanocomposite improves enzyme stability and resistance to inhibitor, International Journal of Biological Macromolecules 105 (2017) 693-701.
[50] M.L. Verma, C.J. Barrow, J.F. Kennedy, M. Puri, Immobilization of β-d-galactosidase from *Kluyveromyces lactis* on functionalized silicon dioxide nanoparticles: Characterization and lactose hydrolysis, International Journal of Biological Macromolecules 50(2) (2012) 432-437.
[51] E. Ranjbakhsh, A.K. Bordbar, M. Abbasi, A.R. Khosropour, E. Shams, Enhancement of stability and catalytic activity of immobilized lipase on silica-coated modified magnetite nanoparticles, Chemical Engineering Journal 179 (2012) 272-276.
[52] C. Pan, B. Hu, W. Li, Y. Sun, H. Ye, X. Zeng, Novel and efficient method for immobilization and stabilization of β-d-galactosidase by covalent attachment onto magnetic Fe_3O_4–chitosan nanoparticles, Journal of Molecular Catalysis B: Enzymatic 61(3-4) (2009) 208-215.
[53] G.A. Drago, T.D. Gibson, Enzyme stability and stabilisation: Applications and case studies, in: m. hofman, p. thonart (eds.), Engineering and Manufacturing for Biotechnology, Springer Netherlands, Dordrecht, 2002, pp. 361-376.
[54] A.A. Homaei, R. Sariri, F. Vianello, R. Stevanato, Enzyme immobilization: an update, Journal of Chemical Biology 6(4) (2013) 185-205.
[55] C. Mateo, O. Abian, R. Fernandez–Lafuente, J.M. Guisan, Increase in conformational stability of enzymes immobilized on epoxy-activated supports by favoring additional multipoint covalent attachment, Enzyme and Microbial Technology 26(7) (2000) 509-515.
[56] H. Fang, J. Huang, L. Ding, M. Li, Z. Chen, Preparation of magnetic chitosan nanoparticles and immobilization of laccase, Journal of Wuhan University of Technology-Mater. Sci. Ed. 24(1) (2009) 42-47.
[57] P.S. Panesar, S. Kumari, R. Panesar, Potential applications of immobilized β-galactosidase in food processing industries, Enzyme research 2010 (2010) 473137-473137.
[58] Q. Husain, S.A. Ansari, F. Alam, A. Azam, Immobilization of *Aspergillus oryzae* β galactosidase on zinc oxide nanoparticles via simple adsorption mechanism, International Journal of Biological Macromolecules 49(1) (2011) 37-43.

Appendices

Supplementary data of this work can be found in online version of the paper

Figure captions:

Scheme 1. Illustrates schematic representation of stepwise preparation of nanobiocatalysts (NBCs) for lactose based dairy industries.

Fig. 1. XRD pattern of **(a)** MWCNT-SnO_2 NCs **(b)** MWCNT-WS_2 NCs**;** Raman spectra of **(c)** MWCNT- SnO_2 NCs and **(d)** MWCNT- WS_2 NCs

Fig. 2.TEM micrograph at resolution of 200 nm **(a)** MWCNTs shows tube within tube like structure **(b)** MWCNT-SnO_2 NCs, SnO_2 NPs attachment on MWCNTs **(c)** MWCNT-WS_2 NCs, nanorods are attached to MWCNTs.

Fig. 3. FE-SEM micrograph at 500 nm **(a)** represents bare MWCNT-WS_2 NCs, WS_2 outgrowth can be seen on MWCNT rods **(b)** shows the enzyme coupled MWCNT-WS_2 NCs dense coverage of enzyme can be seen interconnected MWCNTs rods**(c)** represents the bare MWCNT-SnO_2 in which MWCNT with SnO_2 outgrowth **(d)** white patches of immobilized enzyme onto MWCNT-SnO_2NCs.

Fig. 4 CLSM micrograph of FITC labeled **(a)** Native MWCNT-WS_2 **(b)** *Lcβ-gal* immobilized MWCNT-WS_2 **(c)** Native MWCNT- SnO_2 **(d**) *Lcβ-gal* immobilized MWCNT-SnO_2 at a resolution of 40 μm.

Fig. 5 shows the dependency of *Lcβ-gal* activity in free and immobilized on different NCs *viz* MWCNT-SnO_2, MWCNT-WS_2 **(a)** pH (2.5-7.5) **(b)** temperature (20-70 ℃) **(c)** reusability (9^{th} use) **(d)** storage stability at 4 ℃ under wet condition.

Table 1: Apparent kinetic parameters of free and immobilized enzyme onto MWCNT-WS_2 and MWCNT-SnO_2 NCs.

Scheme 1

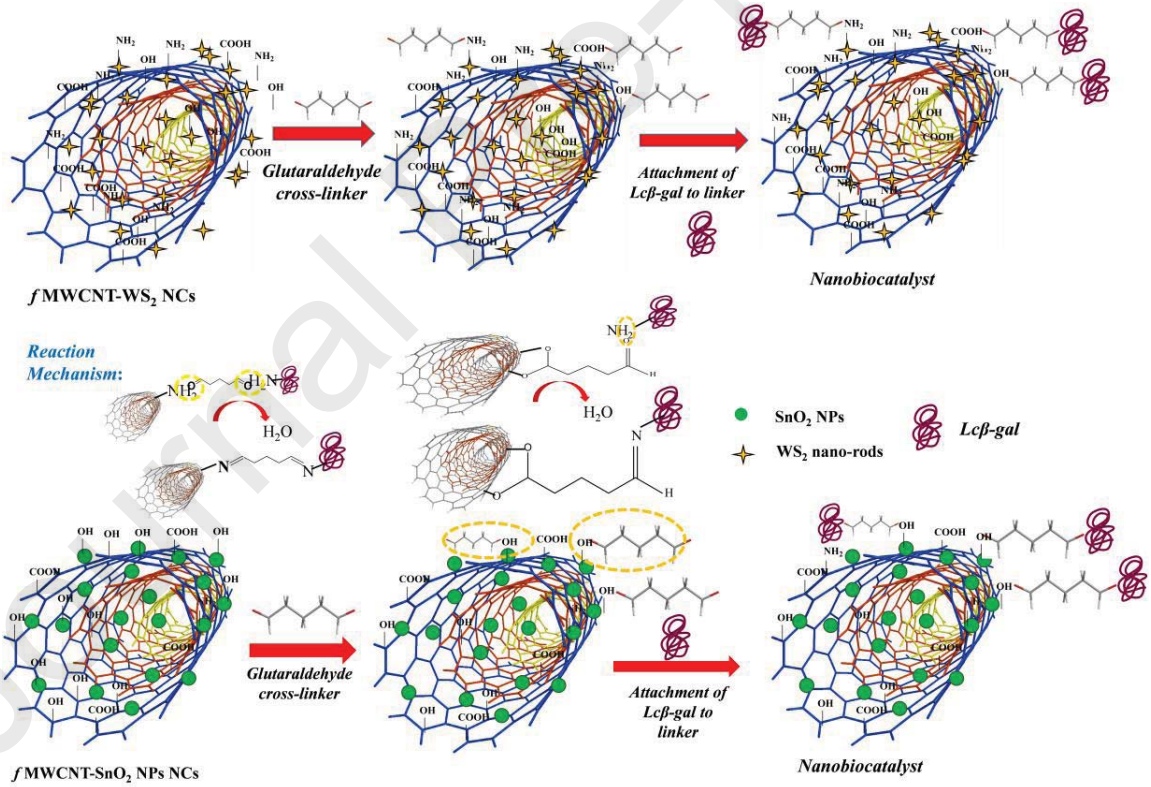
f MWCNT-WS2 NCs
Glutaraldehyde cross-linker
Attachment of Lcβ-gal to linker
Nanobiocatalyst
Reaction Mechanism:
H2O
SnO2 NPs
WS2 nano-rods
Lcβ-gal
f MWCNT-SnO2 NPs NCs
Glutaraldehyde cross-linker
Attachment of Lcβ-gal to linker
Nanobiocatalyst

Fig. 1.

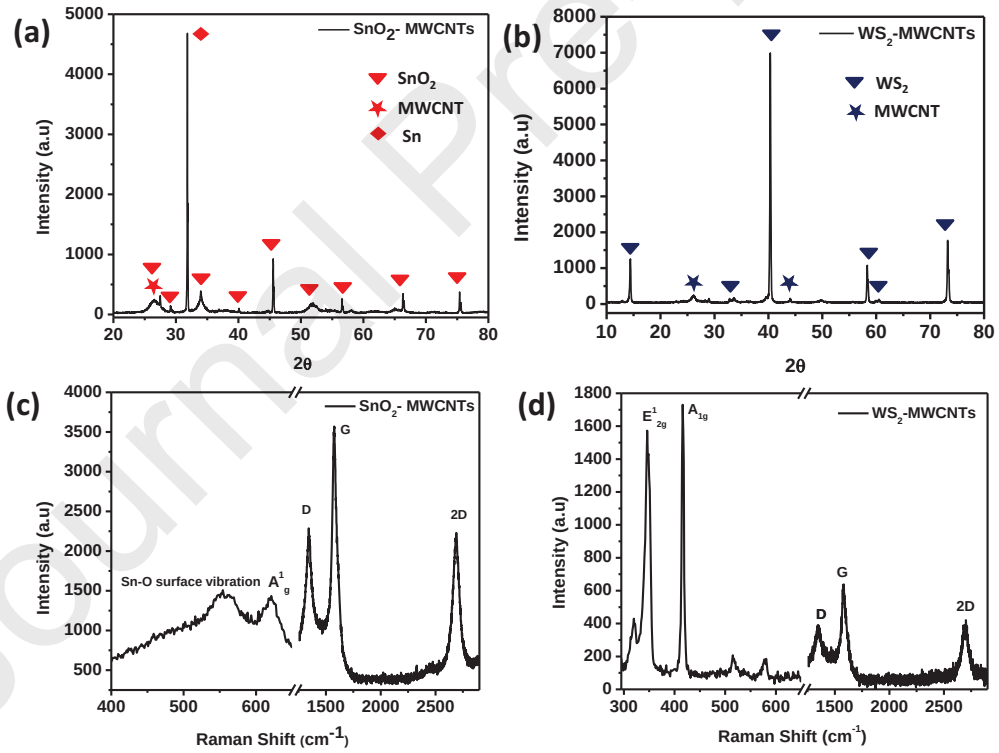

Fig. 2.

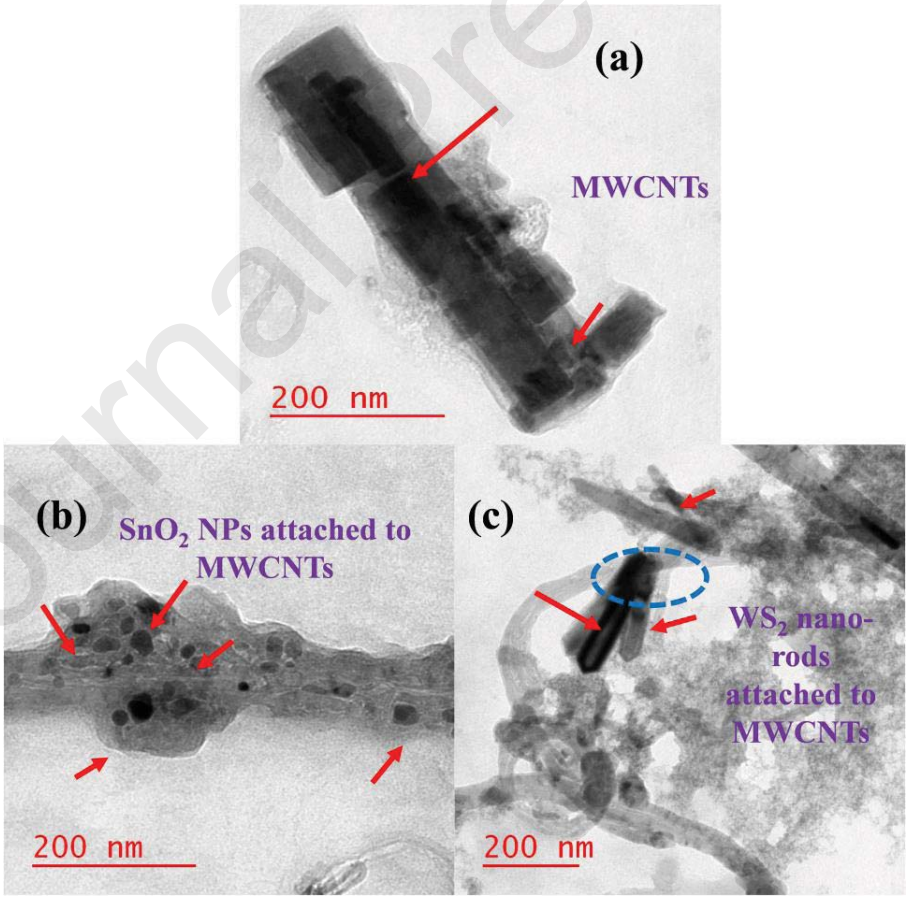
(a)
MWCNTs
200 nm
(b)
SnO_2 NPs attached to MWCNTs
200 nm
(c)
WS_2 nano-rods attached to MWCNTs
200 nm

Fig. 3.

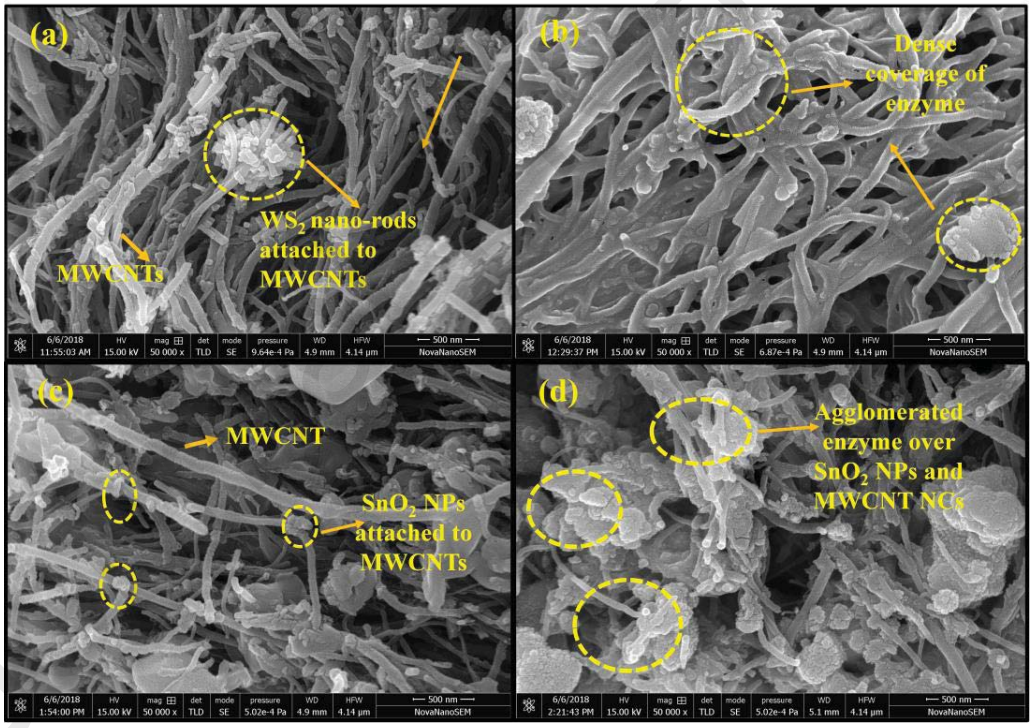
(a)
WS2 nano-rods attached to MWCNTs
MWCNTs
(b)
Dense coverage of enzyme
(c)
MWCNT
SnO2 NPs attached to MWCNTs
(d)
Agglomerated enzyme over SnO2 NPs and MWCNT NCs

Fig. 4.

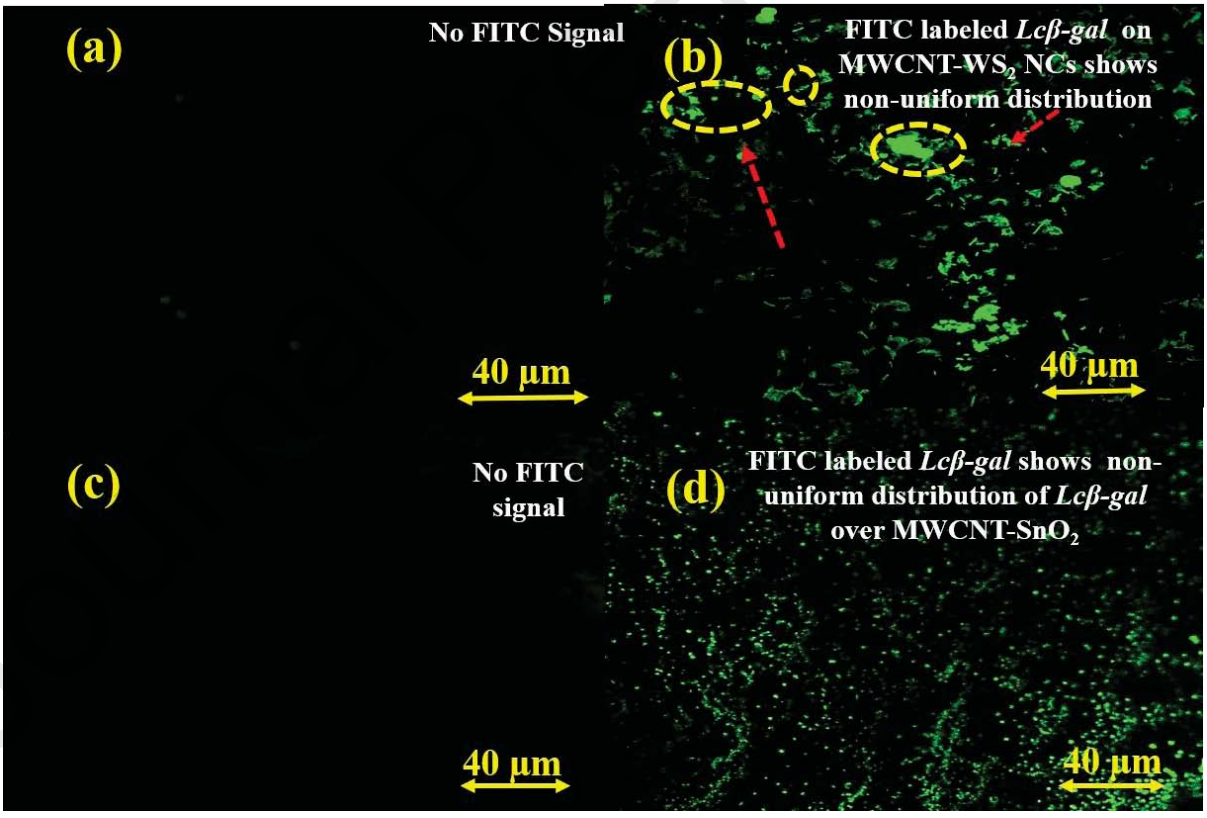
(a)
No FITC Signal
(b)
FITC labeled *Lcβ-gal* on MWCNT-WS_2 NCs shows non-uniform distribution
40 µm
40 µm
(c)
No FITC signal
(d)
FITC labeled *Lcβ-gal* shows non-uniform distribution of *Lcβ-gal* over MWCNT-SnO_2
40 µm
40 µm

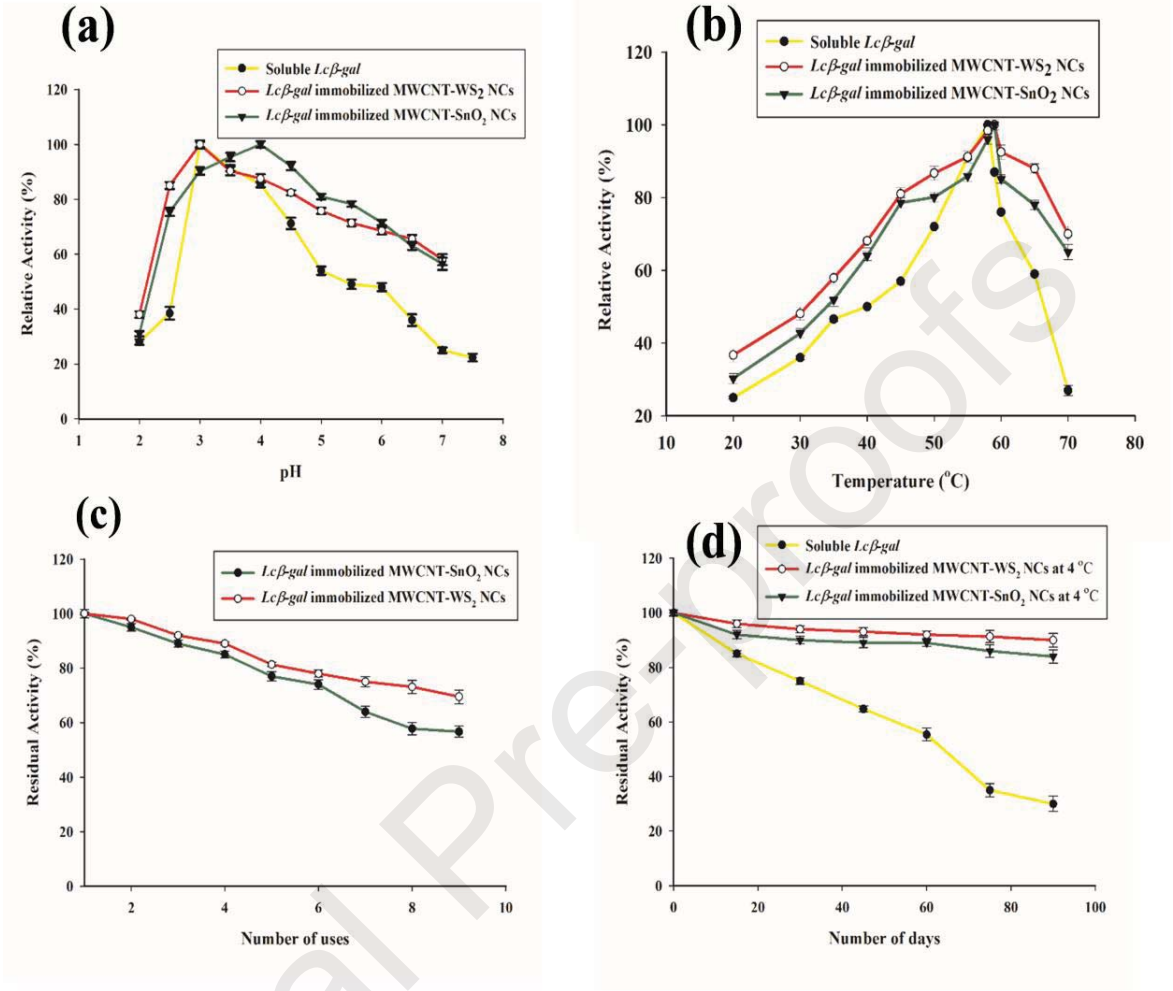

Table 1.

Enzyme preparations	K_m (mM)	V_{max} (μmoles/min/mg)
Soluble *Lcβ-gal*	1.21 ± 0.01	90.90 ± 0.02
Lcβ-gal immobilized onto MWCNT-WS_2 NCs	6.75 ± 0.04	87.80 ± 0.05
Lcβ-gal immobilized onto MWCNT-SnO_2 NCs	5.89 ± 0.03	75.90 ± 0.02

Highlights

- MWCNT-WS_2 and MWCNT-SnO_2 were synthesized *via* eco-facile hydrothermal process.
- The nanocomposites were used to immobilize *Lens culinaris* *β*-galactosidase.
- Storage stability and reusability were superior in MWCNT-WS_2 than MWCNT-SnO_2 NC.
- AFM, FE-SEM, CLSM, and FTIR were employed for characterization of nanobiocatalyst.